ARL-TR-9681 ● MAY 2023

DEVCOM ARMY RESEARCH LABORATORY

On Modeling the Pyrolysis of Hydroxyl-Terminated Polybutadiene (HTPB) Type R45M at Temperatures in the Range 465–600 °C

by Michael J McQuaid, Chiung-Chu Chen, Christopher Stone, and Jeffrey D Veals

NOTICES

Disclaimers

The findings in this report are not to be construed as an official Department of the Army position unless so designated by other authorized documents.

Citation of manufacturer's or trade names does not constitute an official endorsement or approval of the use thereof.

Destroy this report when it is no longer needed. Do not return it to the originator.

ARL-TR-9681 ● MAY 2023

On Modeling the Pyrolysis of Hydroxyl-Terminated Polybutadiene (HTPB) Type R45M at Temperatures in the Range 465–600 °C

Michael J McQuaid, Chiung-Chu Chen, Christopher Stone, and Jeffrey D Veals
DEVCOM Army Research Laboratory

REPORT DOCUMENTATION PAGE

1. REPORT DATE	2. REPORT TYPE	3. DATES COVERED	
		START DATE	END DATE
May 2023	Technical Report	July 2022	January 2023

4. TITLE AND SUBTITLE
On Modeling the Pyrolysis of Hydroxyl-Terminated Polybutadiene (HTPB) Type R45M at Temperatures in the Range 465–600 °C

5a. CONTRACT NUMBER	5b. GRANT NUMBER	5c. PROGRAM ELEMENT NUMBER
5d. PROJECT NUMBER	**5e. TASK NUMBER**	**5f. WORK UNIT NUMBER**

6. AUTHOR(S)
Michael J McQuaid, Chiung-Chu Chen, Christopher Stone, and Jeffrey D Veals

7. PERFORMING ORGANIZATION NAME(S) AND ADDRESS(ES)	8. PERFORMING ORGANIZATION REPORT NUMBER
DEVCOM Army Research Laboratory ATTN: FCDD-RLA-WC Aberdeen Proving Ground, MD 21005	ARL-TR-9681

9. SPONSORING/MONITORING AGENCY NAME(S) AND ADDRESS(ES)	10. SPONSOR/MONITOR'S ACRONYM(S)	11. SPONSOR/MONITOR'S REPORT NUMBER(S)

12. DISTRIBUTION/AVAILABILITY STATEMENT
Approved for public release: distribution unlimited.

13. SUPPLEMENTARY NOTES
ORCID IDs: Michael McQuaid, 0000-0001-5523-7468; Jeffrey Veals, 0000-0002-8238-345X; Chiung-Chu Chen, 0000-0002-8666-9949; Christopher Stone, 0000-0002-9621-5334

14. ABSTRACT
Seeking additional validation of a paradigm for modeling the deflagration of hydroxyl-terminated polybutadiene type R45M that is predicated on the nascent gaseous products of its pyrolysis being represented by 6-ethenyl-2,8,12,16-octadecetetraene (EODT, $C_{20}H_{32}$), we formulated a model for simulating EODT's pyrolysis in T-jump experiments performed by Arisawa and Brill (A&B). The model produced results that raised questions concerning A&B's reduction of their data and some of the conclusions they drew from them. Those findings notwithstanding, the study corroborated A&B's conclusion that the sum of the mass fractions of products with eight or more carbon atoms would approach or exceed 0.50 under the conditions of the experiments. In addition, simulations were performed to predict the degree to which a subsurface layer EODT would decompose prior to reaching the surface of grains burning in opposed-flow diffusion flame (OFDF) experiments. At the low end of the reported burning rates, less than 15 wt% of the starting mass was decomposed at the surface, and at higher burning rates the percentages were less. As such, they provided further evidence that EODT is more representative of the gaseous products desorbing from the surface of R45M strands burning in OFDF experiments than 1,3-butadiene.

15. SUBJECT TERMS
Weapons Sciences, R45M, hydroxyl-terminated polybutadiene, HTPB, chemical kinetics, pyrolysis, modeling

16. SECURITY CLASSIFICATION OF:			17. LIMITATION OF ABSTRACT	18. NUMBER OF PAGES
a. REPORT	b. ABSTRACT	C. THIS PAGE		
UNCLASSIFIED	UNCLASSIFIED	UNCLASSIFIED	UU	42

19a. NAME OF RESPONSIBLE PERSON	19b. PHONE NUMBER *(Include area code)*
Michael McQuaid	(410) 278-6185

STANDARD FORM 298 (REV. 5/2020)
Prescribed by ANSI Std. Z39.18

Contents

List of Figures

List of Tables

Acknowledgments

We are grateful to Dr Claresta Dennis (Naval Air Warfare Center Weapons Division China Lake) for providing measured values for R45M's density as a function of temperature. Funding for this study was provided by the DEVCOM ARL mission program "Modeling and Experimentation for Propellants."

1. Introduction

Hydroxyl-terminated polybutadiene (HTPB) type R45M is widely employed as a binder for composite propellants and explosives. The first two authors' interest in modeling its pyrolysis and combustion dates to 2008 (Chen and McQuaid 2009). Collaborating with US Army Combat Capabilities Development Command (DEVCOM) Aviation & Missile Center researchers to develop a hypergolic hybrid (HH) rocket motor concept whose fuel grain included R45M as an ingredient (Wingard et al. 2010), they were responsible for constructing a detailed gas-phase finite-rate chemical kinetics mechanism for a computational fluid dynamics (CFD) model with which to simulate the concept's combustion chamber dynamics (Nusca et al. 2011). At that time the most advanced models for simulating HTPB's deflagration prescribed a "light hydrocarbon" such as ethylene (C2H4)* (Cai et al. 2008) or 1,3-butadiene (C4H6) (Gross 2007) as the (only) nascent gas-phase product desorbing from burning surfaces. Intuiting that such constructs might not produce reliable results for regions in the HH combustor where thermal loads and/or oxidizer concentrations were low, they proposed prescribing the notional molecule 6-ethenyl-2,8,12,16-octadecetetraene (EODT) instead. The rationale for this prescription was that, although the pyrolysis of R45M might not produce EODT ($C_{20}H_{32}$, 272 amu) in significant concentrations (if at all), being 1/9th the size of nominal R45M polymer chains and having the same nominal ratio of cis:trans:vinyl butadiene monomers as those chains, it would decompose much like R45M. As such, it was considered likely that a comprehensive mechanism for modeling its combustion would offer a better representation for the gas-phase reaction chemistry driving R45M's deflagration than one that was only suitable for modeling C2H4's or C4H6's.

Toward creating a mechanism for decomposing and combusting EODT, the second author employed quantum-mechanics-based electronic structure methods to characterize minimum energy paths (MEPs) for a variety of potentially relevant ene/retro-ene and simple bond scission reactions that had been postulated to be important first steps in the decomposition of HTPB/R45M (Chen and McQuaid 2009). Those results were employed to parameterize formulae for computing the thermodynamic properties of the MEP's local minima and transition states. Transition state theories were then employed to parameterize rate coefficients (k_i^{rxn}) for elementary gas-phase reactions (i).

*The labels given to some molecules in this report indicate their stoichiometry but will be observed to deviate from a conventional stoichiometry-based label (e.g., "C_2H_4" for ethylene). That is intentional. The labels given correspond specifically to the molecule's label in the detailed finite-rate chemical kinetics mechanism employed for the study.

To assess the resulting formulary's potential to represent R45M's pyrolysis when it was first assembled, the k_i^{rxn} for all the unimolecular reactions that decomposed EODT were summed at selected temperatures (T) from 280 to 730 °C and compared to global rate coefficients for gasification [$k_G^g(T)$] derived from measured mass loss versus time data that were published in the open literature (Varney and Strahle 1971; Ericsson 1978; Du 1989; Chen and Brill 1991; Arisawa and Brill 1996a,b; Lu and Kuo 1996).* It was observed that the sums fell near the middle of the measured $k_G^g(T)$ values. Particularly relevant to the study summarized herein, the sums were observed to be in good agreement with $k_G^g(T)$ values Arisawa and Brill (A&B) derived from spectroscopically based measurements of the temporal evolution of gas-phase species concentrations produced by R45M's flash pyrolysis in "T-jump" experiments (A&B 1996a,b).

The creation of a mechanism for modeling EODT's gas-phase combustion when mixed with red fuming nitric acid (RFNA) followed (Chen and McQuaid 2010). That construct was further expanded to include formulary developed to create mechanisms suitable for modeling the decomposition and combustion of composite solid propellants and explosives (Chen and McQuaid 2011, 2015; Veals et al. 2019). An effort to develop a CFD model for simulating the combustion chamber dynamics of solid-fuel ramjet (SFRJ) combustors having (neat) R45M fuel grains motivated the inclusion of formulary necessary to model EODT's O_2-promulgated combustion (Chen and McQuaid 2020). Considered suitable for modeling both HTPB/R45M-air and HTPB/R45M-RFNA combustion, the "EODT–RFNA–air" mechanism comprised more than 1300 species and 5400 elementary reactions when the study summarized herein commenced.

Over the 14+ years the EODT–RFNA–air mechanism has been developed and applied, we have not observed it to produce any results that have caused us to question the basic premise that was the initial motivation for its creation (i.e., that EODT's gas-phase decomposition and combustion would be more representative of the reaction chemistry driving R45M's deflagration than a light hydrocarbon's). However, the primary tests of the paradigm's validity have been 1) the seeming reasonableness of CFD simulations performed with skeletal versions of it, and 2) comparisons of measured and predicted burning rates for composite energetic materials in which R45M only comprised up to 20 wt%. Evaluations based on comparing physics-based model predictions to measured data that are generally more difficult to reproduce, such as the concentrations of species evolved from

* Chen and McQuaid (2009) state that CHEMKIN was employed to simulate bulk-phase decomposition of R45M as a function of temperature. That statement, which was added by the first author (MJM) of this report and unnoticed at the time by that paper's first author (CCC), is not correct.

pyrolyzed and/or deflagrating samples, were not conducted. In the case of modeling R45M's pyrolysis, they were not attempted because we were unaware of any established frameworks offering reasonable representations for the experiments that had generated such data, and at the time we did not have the wherewithal to develop them ourselves.

The motivation for the study summarized herein was twofold. One was ongoing DOD-wide efforts to develop SFRJs for tactical missile applications (Chen and McQuaid 2020). Fuel grains formulated with (neat) R45M are serving as prototypes for these efforts. And given R45M's already ubiquitous employment as a binder for composite propellants and explosives, we expect it will be employed in attempts to formulate higher performing composite SFRJ fuel grains (Sandall et al. 2017). CFD models are being developed and applied to gain insights that will advance the technology (Nusca et al. 2019, Nusca 2022), and as in the effort to develop a CFD model for simulating the HH combustor concept that led us to propose prescribing EODT as the nascent product of R45M's pyrolysis in deflagration models, the reliability of their predictions for performance at off-design conditions will likely depend critically on the validity of their representation for R45M's pyrolysis and combustion.

Recognizing this importance, researchers at Purdue University (McDonald et al. 2023) and Navy laboratories (Geipel et al. 2022) have conducted relevant counter-flow burner experiments and measured regression rates as well as temperature and species concentrations as a function of distance above the burning surface, affording tests of the schema. However, deflagration processes as a whole largely follow from processes that occur within 10 microns of the burning surface (Chen et al. 2019) and the spectral probes employed for the latter measurements had/have little to no capacity to generate reliable data in this region. It was envisioned that a modeling-based study of R45M's pyrolysis could help bridge that gap.

In addition, we had theorized a framework for modeling condensed-phase reaction chemistry (Veals et al. 2018) that (we hoped) offered a reasonable representation for simulating R45M's pyrolysis. Predicated on estimating rate coefficients for elementary condensed-phase reactions by multiplying the rate coefficients for analogous gas-phase reactions by a probability function derived from free-volume theory, the framework had been applied to model the decomposition of liquid nitroglycerin and showed promise (McQuaid et al. 2021). Seeking additional validation of the framework and recognizing that "more is known about HTPB than any other binder/fuel" (A&B 1996a), we believed demanding tests of both the EODT mechanism and the theorized framework for modeling condensed-phase reaction chemistry could be found in the corpus related to HTPB's pyrolysis.

Of the many published measurement-based techniques employed to study HTPB's pyrolysis, A&B's T-jump experiments (A&B 1996a,b) had several attributes that made them an attractive test case. For one, they involved relatively high (≥100 °C/s) heating rates and were conducted at somewhat elevated pressure (P = 2 or 11 atm). As discussed by A&B, the process by which R45M pyrolyzes is a function of these two parameters, and the values established in their T-jump experiments were considered likely to be similar to those that R45M would experience in propulsion-relevant deflagration scenarios. In addition, A&B employed Fourier transform infrared (FTIR) spectroscopy to measure in near-real-time the concentrations of gas-phase products "desorbed"* from the condensed phase, and these data offered direct tests of the mechanism's capacity to represent the reaction chemistry effecting R45M's pyrolysis.

Several of A&B's conclusions warrant mentioning here. Observing that the gasification rates of products/species (j) were relatively steady when their concentrations were observable and rising, A&B converted measured rates into rate coefficients $\left(k_j^g\right)$ based on the assumption that the kinetics of the gasification process were zeroth order. That being at odds with our expectations and results generated by the model we formulated to simulate the experiments, we worked through A&B's approach to reducing their data to ensure we understood what they had done. That effort proved instructive, revealing that the $k_j^g(T)$ values A&B reported corresponded to maximum gasification rates that were far from representative of the processes' kinetics as a whole. As such, in isolation they would yield poor predictions for the extent to which R45M would pyrolyze when subject to the thermal transients to which it would be subject in deflagration scenarios.

*A&B employed the term "desorption" to describe the process by which R45M's pyrolysis products gasified. This term generally bespeaks a physical process in which an adsorbed substance is released from a (solid) surface, and the model A&B formulated to interpret their data is consistent with this conceptualization of the process. Given that the samples were liquids, we imagined the process being more like evaporation than desorption. And were we to develop a physics-based model for predicting gasification rates (in g/s), we would formulate it based on that conceptualization. As undertaken to create a model for simulating accelerating rate calorimetry experiments (McQuaid et al. 2017), it would involve formulating equations to compute the sample's surface area (in cm^2) and the mass flux (in g/cm^2s) from that surface. To the extent models of desorption and evaporation both predicate mass transfer occurring only at a mechanically quiescent interface between the condensed and gas phases, the primary difference between them is the formula(e) employed to compute the mass flux from the surface. From the standpoint of comparing the results and conclusions derived from the models formulated and applied by A&B and by us, that difference is irrelevant. In both cases, coefficients for computing desorption/evaporation rates were specified heuristically, and therefore the differences between the conclusions drawn from the two studies are not ascribable to the different conceptualizations. Therefore, to avoid confusion in the discussion that follows, the gasification process is also referred to herein as desorption.

As is discussed in detail in Section 4.1, maximum model-predicted $k_G^g(T)$ values

$$k_G^g(T) = \sum_j^J Y_j^\infty k_j^g(T) \quad (1)$$

where Y_j^∞ was the mass fraction of j at the end of the simulation, were found to be within a factor of 2 of the $k_G^g(T, 2\text{ atm})$ values reported by A&B over the entire temperature range considered (465 °C ≤ T ≤ 609 °C) if the rate coefficients for desorption (k_j^d) had values above a certain magnitude. However, the slope of the model-predicted $k_G^g(T)$ versus T^{-1} plots did not exhibit the break observed in the measurement-based $k_G^g(T, 2\text{ atm})$ versus T^{-1}plot unless k_j^d values were set below this level.* In addition, no model-predicted $k_G^g(T)$ versus T^{-1} plots reasonably reproduced A&B's measurement-based $k_G^g(T, 11\text{ atm})$ versus T^{-1}plot.

The slope break in the $k_G^g(T, 2\text{ atm})$ versus T^{-1} plot A&B (1996b) derived from their data led them to conclude the following:

> [F]or the purpose of modeling the binder pyrolysis rate during combustion of solid rocket propellants containing HTPB, the desorption kinetics involving higher molecular weight fragments should be employed rather than the bulk-phase chemical decomposition kinetics.

Consistent also with results published by Ganesh (2000), results produced by our model corroborated A&B's conclusion regarding the relative importance of "higher" molecular-weight products. However, the discrepancies noted led us to question A&B's and our conceptualization of the mass transfer process (i.e., desorption/evaporation via a mechanically quiescent free surface). Indeed, they led us to conclude that, like a pot of water on a hot plate, gasification rates adjacent to the heated surface likely exceeded those at the free surface, producing a bubble field that was a major source of the gas eluted into the probe volume. However, even if that was not the case, the modeling results made clear that the kinetics of desorption/evaporation and bulk-phase chemical kinetics are not separable in the manner prescribed by A&B's model of the process. Among other things, mass transfer rates at an interface are generally a function of molecular size, and chemical kinetic rates dictate how long it will take to produce sizes that will readily gasify at a given temperature. We also note that A&B heated the samples via a platinum (Pt) filament that was in direct contact with them, and Pt is known to catalyze hydrocarbon cracking (Myers and Munns 1958). Therefore, one should be cautious in using A&B's results as a basis for parameterizing an R45M deflagration model.

*Appreciating that it might be confusing to the reader, we note that k_j^d and k_j^g are different parameters. The k_j^d were user-specified parameters of our model. The k_j^g, which were derived from species concentration versus time plots, were a function of k_j^d and $\{k_i^{rxn}\}$.

To the extent we believe bubble-promulgated mass transfer played an important role in A&B's T-jump experiments, the value of the experiment's results for validating our paradigm for modeling R45M's deflagration and our framework for representing condensed-phase reaction kinetics was limited. Nonetheless, comparisons of model-predicted and measurement-derived results suggested that the subset of the EODT–RFNA–air mechanism that was integrated with the model offered a reasonable representation for the reaction chemistry. In addition, believing that bubble-promulgated mass transfer is much less likely to play an important role in laminar deflagration scenarios, such as those realized in opposed-flow diffusion flame (OFDF) experiments (Geipel et al. 2022; McDonald et al. 2023), we performed simulations to predict the extent to which a subsurface layer of R45M will decompose prior to reaching the burning surface. The simulations indicated that a relatively small fraction of R45M's intramolecular bonds will be broken prior to its gasification, suggesting that EODT is far more representative of the nascent gaseous products at the surface of an R45M strand burning in an OFDF experiment than a light hydrocarbon. Moreover, since the degree of decomposition was inversely proportional to the burning rate, and burning rates are expected to be higher in SFRJ combustors, that conclusion extends to CFD models for simulating their dynamics as well.

2. A Review of A&B's T-jump Experiments and Data Reduction Approach

A&B presented a relatively detailed description of the T-jump experiments they conducted with R45M. We restate here those aspects of the experiments that were bases for formulating a homogeneous reactor (HR) model for simulating them. Also reviewed is the method A&B employed to reduce the (raw) data their experiments generated. Some symbols employed by them have been changed to conform to our preferences.

2.1 T-jump Experiment Procedures

In the T-jump experiments A&B performed with R45M, an approximately 0.2-mg (200-μg) sample was spread as a (liquid) film about 100 μm thick on the center of a Pt ribbon filament. The filament was housed in a gas-tight spectroscopic cell filled with cool (approximately 25 °C) static argon (Ar). (The volume of the cell was not provided.) Targeting a specified final/hold temperature (T_{hold}) in the range 465–609 °C, A&B estimated that the nominal rate at which samples were heated was approximately 600 °C/s. The time (t) necessary to reach T_{hold} was therefore 0.7–1 s. The experiments' durations were reported to be 19 s.

The concentrations of gas-phase species were measured via FTIR spectroscopy approximately 0.3 cm above the sample's surface. A&B summarized the quantitation of the raw spectral data into species concentrations (C_j), and we did not identify any obvious flaw in their approach. However, based on our (limited) experience in measuring C_js using optical spectroscopies (McQuaid et al. 1991; McQuaid et al. 2002), we had concerns about the accuracies of these measurements. Measurements of absolute concentrations in real time in an evolving complex mixture can be impacted by many factors. Regardless, finding no specific reason to question their $C_j(t)$ measurements, we conducted our evaluation assuming they were accurate.

In addition to measuring the temporal evolution of various C_j, A&B obtained an indication of whether the pyrolysis process absorbed or released heat by measuring the difference between the voltage required to heat the sample-filament system and that needed to heat the filament alone. In the one plot of such data that they presented (see Fig. 13 in A&B-I [A&B 1996a]), the process was endothermic (i.e., absorbed heat) during the first 3 s of the experiment, then was exothermic for about 4 s before asymptotically approaching thermoneutral.

2.2 Reduction of Measured Species Concentration Data

From the standpoint of mechanism–model validation, the measurement-based data that were of most interest to us were the $k_j^g(T)$ values A&B derived for the six major products to which they attributed features of spectra generated by their FTIR probe. However, as mentioned in the introduction, A&B's approach to deriving $k_j^g(T)$ presumed behavior at odds with our expectations. As summarized in Section III.A of A&B-II (A&B 1996b), A&B observed that for temporal intervals of 0.5–2 s during which C_js were observable and increasing, the increases as a function of time (t) were nearly linear. Therefore, they employed a zeroth-order representation to reduce the data, computing k_j^g per

$$k_j^g(T_{hold}) = \frac{d\left(C_j(T_{hold},t)/C_j^\infty\right)}{dt} \tag{2}$$

where in an experiment performed at a given T_{hold}, $C_j(T_{hold},t)$ was j's concentration at time t, and C_j^∞ was its concentration at the end of the experiment. A&B also stated that "for convenience" they employed $C_j^\infty = C_j^\infty$ (609 °C) for calculating $k_j^g(T_{hold})$ regardless of T_{hold}'s value.

Our reason for questioning A&B's approach to reducing their data was our expectation that gasification rates would decrease with a decrease in the sample's mass (m_c). Indeed, A&B reported that 90%–95% of the samples' initial masses

(m_0) gasified in experiments with T_{hold} values in the range 400–500 °C and that the percentages were higher at higher T_{hold} values. Thus, we expected gasification rates would exhibit the characteristics of a first-order kinetic process and be analyzed as such. Noting that Ericsson (1978) had observed the kinetics of C4H6 formation produced by the pyrolysis of cis-1,4-polybutadiene at heating rates comparable to T-jump experiments to be first order, A&B attributed the difference to the difference in the sizes of the samples in the two studies. They considered the results produced with the larger samples employed in their experiments likely to be more representative of R45M's pyrolysis in deflagration scenarios because in those scenarios the concentration of the polymer remained relatively constant.

Attempting to reconcile A&B's data reduction approach and our expectations, we worked through A&B's derivation of $k^g_{C4H6}(T)$ values to verify that we understood what they had done. That proved to require several steps. First, although A&B's use of Eq. 2 to derive $k^g_{C4H6}(T_{hold})$ from "processed" $C_{C4H6}(480\ °C, t)$ data presented in Fig. 3 of A&B-II (A&B 1996b) appeared straightforward, a side-by-side comparison of the processed data with the "raw" $C_{C4H6}(480\ °C,\ t)$ data presented in Fig. 2 of A&B-II was not sufficient to convince us that there was a one-to-one correspondence between the two. Therefore, we digitized the data in the two figures using DataThief (Tummers 2006) and plotted them in one graph. As shown in Fig. 1 (herein), the $C_{C4H6}(480\ °C, t)$ data in A&B-II Fig. 3 overlapped the $C_{C4H6}(480\ °C, t)$ data in A&B-II Fig. 2 when the former was shifted 6.3 s later in time. As such, it addressed that concern but also revealed that Eq. 2 was not at all representative of the rate of the process as a whole. From a chemical kinetics viewpoint, the approximately 4-s interval between the time the sample first reached T_{hold} and C_{C4H6} was observed as well as the rate increase from 4 to 6 s is germane to modeling the temporal evolution of the process.

Next, we sought to confirm that the $k^g_{C4H6}(T_{hold})$ data presented in Fig. 5 of A&B-II (A&B 1996b) could be derived from the $C_{C4H6}(T_{hold}, t)$ data presented in Fig. 3 of A&B-II. However, A&B did not report $C^{\infty}_{C4H6}(609\ °C)$. To estimate it we employed the parameters of the Arrhenius expression presented in Fig. 3 of A&B-II [$\ln(A/s^{-1}) = 11$; $E_a = 19$ kcal/mol] to calculate $k^g_{C4H6}(609\ °C)$ ($1.17\ s^{-1}$) and we employed a digitization of the $C_{C4H6}(609\ °C, t)$ data in Fig. 3 of AB-II to compute $dC_{C4H6}(609\ °C, t)/dt$ (1.99×10^{-4} mol/l-s). Combined, they implied $C^{\infty}_{C4H6}(609\ °C)$ was 1.7×10^{-4} mol/l. Computing $k^g_{C4H6}(T)$ at 465, 480, 500, 530, 557, and 580 °C based on this value and the $dC_{C4H6}(T_{hold}, t)/dt$ values derived from the $C_{C4H6}(T_{hold})$ versus *t* plots in Fig. 3 of AB-II, we found as shown in Fig. 2 (herein) that they were in good agreement with values computed with the Arrhenius expressions A&B had derived to represent the $k^g_{C4H6}(T_{hold})$ data, confirming that this was their approach to reducing the raw measured data.

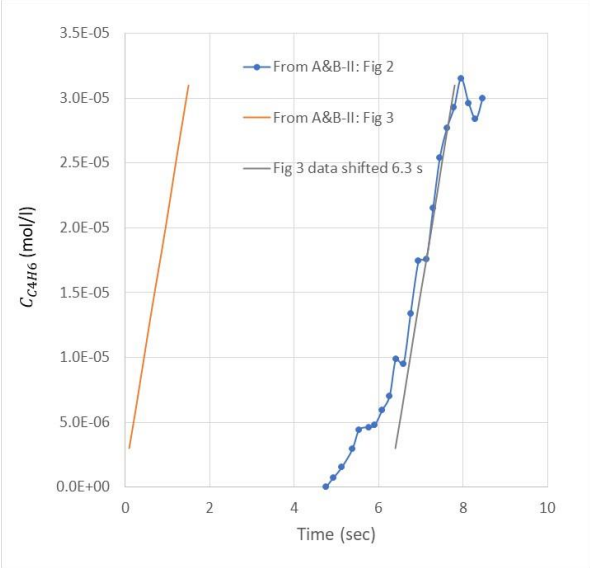

Fig. 1 Confirmation of the manner in which A&B processed raw $C_j(T_{hold}, t)$ vs. t data

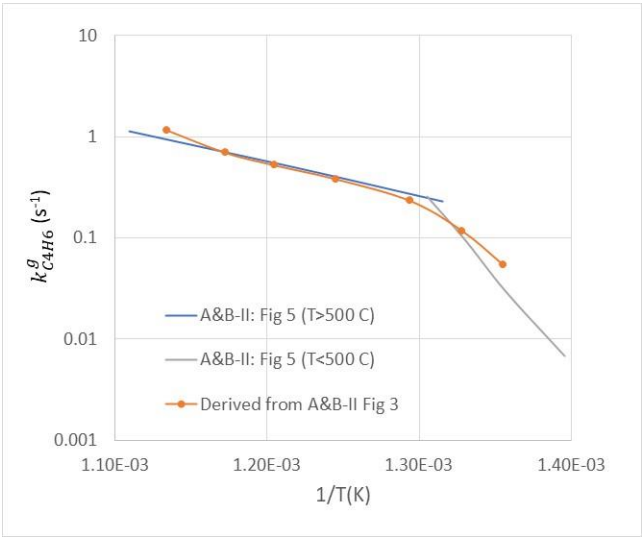

Fig. 2 Confirmation of the basis for A&B's approach to reducing their data

Although those results reassured us that we understood how A&B had reduced their data, the fact that Eq. 2 was not representative of the gasification process from start to finish meant that the $k_j^g(T_{hold})$ values A&B reported were different from those a standard chemical kinetics analysis would produce. However, the time delay between the onset of heating and the first detection of products that might have enabled such an analysis was only reported for one case. (See Fig. 13 of A&B-I [A&B 1996a], which is partially reproduced in Fig. 1 herein.) As such, we could only speculate as to what the delays were at different T_{hold} and/or P values. We presumed delays would increase with a decrease in T_{hold}, and thus suspected that the gasification rates at lower T_{hold} values as represented by the published

$k_j^g(T_{hold})$ and $k_G^g(T_{hold})$ values might be overstated relative to those at higher T_{hold} values. The ramifications of this (presumed) bias are discussed in Section 4.1.

To compare model-generated $C_j(t)$ predictions to plots presented by A&B, we also needed to know the volume (V) of the gas in the spectroscopic cell. As already mentioned, that volume was not reported. In a T-jump-based study published by Brill (1994) prior to A&B-I/II (A&B 1996a,b), its value was 25 cm^3, and we presumed that was its value in the experiments of interest. However, before finding that information, we estimated V based on the observation in A&B-I (A&B 1996a) that the mass fraction of C4H6 at the end of the experiment(s) at 609 °C was 0.151. Since nominal m_0 values were 200 μg, this implied that the mass of C4H6 at the end of the experiment was approximately 30 μg (5.6×10^{-7} moles). Therefore, having found that C_{C4H6}^{∞}(609 °C) was approximately 1.7×10^{-4} mol/l, this implied V was approximately 3.3 cm^3. Thus, we had some concerns about the self-consistency of the data reported by A&B. As is discussed in Section 4.3, shortcomings of the model prevented it from providing insight into the matter.

3. Modeling Considerations

3.1 The Finite-Rate Chemical Kinetics Mechanism

Since we were only interested in modeling HTPB/R45M's pyrolysis (in the absence of an oxidizer), we stripped from the EODT-RFNA-air mechanism all species and reactions that involved any atoms other than carbon or hydrogen. The resulting network comprised 304 species and 1018 reactions. All the data composing this mechanism are provided in an addendum to this report (Chen et al. 2023).

3.2 The Homogeneous Reactor Model

The HR model we formulated to simulate the T-jump experiments was a variation of the HR model we formulated to simulate the decomposition of closed, constant-volume, 2-phase nitroglycerin systems (McQuaid et al. 2021). Figure 3 is provided to afford a sense for the dimensions of the experiment's components. The model was predicated on the sample being monolithic and having a volume that was negligible compared to the fixed volume of the gas-tight cell surrounding it. It also predicated the sample being uniformly heated by the filament. Gases produced by pyrolysis only desorbed from the sample's free surface and instantaneously and homogenously occupied the entire gas-phase volume. Gasification caused a reduction in the sample's volume (V_c) and the area of its free surface (SA_c). Because V_c was negligible relative to the gas phase's volume (V), the increase in V due to

V_c's reduction was deemed insignificant and the calculation of species' concentrations did not account for it.

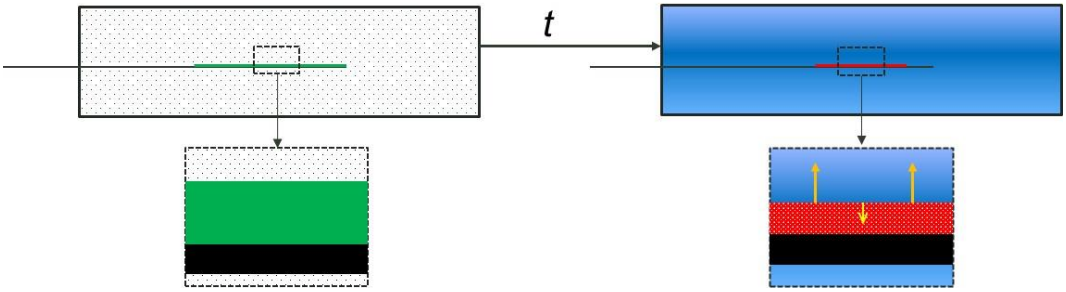

Fig. 3 Considerations in formulating an HR model for simulating T-jump experiments

The reduction in SA_c with the reduction of the sample's mass (m_c) (of course) depends on the sample's shape/topology. Beyond knowing that the samples were liquid films about 100 μm thick, we were left to speculate. Relevant to this issue, the parameter in A&B's model that corresponded to SA_c was a constant and therefore represented a scenario in which the sample's SA_c/V_c increased during the course of an experiment. Being somewhat skeptical of that possibility (for a sample in which bubbles did not form), we settled on making SA_c proportional to m_c. While this would only be strictly true for a shape whose SA_c/V_c remained constant as m_c decreased, as is discussed in Section 4.1, the k_G^g predictions that were ultimately compared to measurement-based values corresponded to times when the amount of decomposition was low. Therefore, we believed the dependence of SA_c on m_c would have had to have been significantly different from the one prescribed to obviate the conclusions drawn from the model's k_G^g predictions.

Consistent with this conceptualization of the process, the desorption rate of each species $\left(r_j^d\right)$ was computed per

$$r_j^d = \alpha_j k_j^d m_j \tag{3}$$

where m_j was species j's mass and α_j was its (dimensionless) "anti-sticking" coefficient.* Only temperature-independent constants were specified for both α_j

*Our use of α_j in formulae for computing mass transfer rates at the interface between condensed and gas phases began with the incorporation of a Hertz–Langmuir–Knudsen (HLK) relationship into a model for simulating accelerating rate calorimetry experiments (McQuaid and Chen 2017). Following from an HLK representation employed by Miller (1997), that relationship included a parameter "α" that he referred to as a "sticking" coefficient. That name presumably came from the vernacular of surface physics, where the parameter quantifies the ratio of the number of atoms or molecules that adsorb/stick to a surface to the total number that impinge on it. Per this definition, α is set equal to 1 when all molecules impinging on the surface are expected to stick, preventing (re)gasification. In our model, α_j has the opposite sense. An α_j equal to 1 presumes species j cannot stick and therefore desorbs at the maximum possible rate ($k_j^d m_j$).

and k_j^d. Summed, the r_j^d yielded the temporal rate of change of m_c:

$$\frac{dm_c}{dt} = -\sum_{j=1}^{J} r_j^d. \quad (4)$$

Formulated in terms of species mass fractions (Y_j)

$$Y_j = \frac{m_j}{m_c}, \quad (5)$$

Equation 4 became

$$\frac{dm_c(t)}{dt} = -m_c(t) \sum_{j=1}^{J} \alpha_j k_j^d Y_j(t). \quad (6)$$

Formulating the species conservation equations in terms of Y_j, we obtained

$$\frac{dY_j}{dt} = \frac{P_{HFV} \dot{\omega}_j W_j}{\rho_c} + Y_j \left[\left(\sum_{j'}^{J} \alpha_{j'} k_{j'}^d Y_{j'} \right) - \alpha_j k_j^d \right] \quad (7)$$

where P_{HFV} is a function for computing the probability that potential reactants are proximate to a free-volume hole that is large enough for their reaction to occur (and concomitantly prevented from reversing) (Veals et al. 2018; McQuaid et al. 2020), $\dot{\omega}_j$ is the molar production rate of the *j*th species, W_j is its molecular weight, and ρ_c is the condensed-phase's density. The temperature of the condensed phase was programmed to reproduce A&B's characterization of the heating protocol employed for the experiments (i.e., ramped (linearly) from 25 °C to T_{hold} at 600 °C/s, then fixed at T_{hold} for the duration of the simulation). The durations of the simulations were specified so that m_c values decreased to less than $0.01 m_0$. Because the gas phase in the experiments was approximately 25 °C, we assumed (as did A&B) that reactivity in that phase could be neglected.

We note that in A&B's model of the process, they employed a function to represent the desorption process (i.e., $\theta N_0 k_s$ in A&B-II [A&B 1996b]) that was conceptually different from Eq. 3. However, in both studies, the values of the parameters in their respective functions were specified heuristically. Therefore, from the standpoint of simulating the experiments, the difference between them was irrelevant. However, A&B also supposed that m_c (i.e., *M* in A&B-II [A&B 1996b]) was a constant. That prescription, which is clearly at odds with the results of their experiments, effectively decouples the chemical kinetics from the desorption kinetics. Perhaps more important than our model including a detailed finite-rate chemical kinetics mechanism to represent the reaction chemistry, that difference was a significant factor in the difference in the trends in the gasification rates predicted by the two models and (consequently) the conclusions drawn from them.

As in a prior study (McQuaid et al. 2021), the basis to employ for computing ρ_c was an issue because we were unaware of any practical approach for accurately estimating it for a decomposing condensed phase. Assuming it would be effectively independent of the gas phase's pressure and that it would not be significantly lower than extrapolations of values for neat R45M that were measured at lower temperatures (Dennis 2021), it was computed (in g/cm^3) per

$$\rho_c = 1.0524 - 0.0005T \tag{8}$$

where T was in K.

In addition, being skeptical of A&B's finding that the pyrolysis process exhibited exothermicity, we presumed the relative enthalpies of the species in the condensed phase ($\Delta h^c_{j-j'}$) would be similar to their gas-phase counterparts $\left(\Delta h^g_{j-j'}\right)$ and computed an instantaneous rate of heat release $(\dot{q})$ per unit mass per

$$\dot{q} = -\frac{\sum_j^J P_{HFV}\dot{\omega}_j h_j^g}{\rho_c}. \tag{9}$$

(Given that all the species except H and H_2 were hydrocarbons, we doubted intermolecular interactions would significantly change their enthalpies relative to one another.) We note that per this definition, $\dot{q} > 0$ values were generated when (cumulatively) chemical reactions were "releasing" energy (rather than absorbing it), indicating the process as a whole was exothermic.

4. Results

4.1 Global Gasification Rates

A&B derived $k_G^g(T_{hold})$ values from $k_j^g(T_{hold})$ values they had measured for the six major gaseous products detected by FTIR. (They do not specifically state how they derived the former from the latter, but based on the definition of the former, we assume it was a Y_j^∞-weighted sum, viz. Eq. 1.) The results are presented in Fig. 8 of A&B-II (A&B 1996b). (The Arrhenius expressions that A&B fit to the $k_G^g(T,P)$ values are reproduced in Fig. 5 herein.) In A&B's $k_G^g(T_{hold}, 2\text{ atm})$ versus ${T_{hold}}^{-1}$ plot, a distinct break in the slope was observed at approximately 530 °C. As mentioned in the introduction, A&B attributed the break to a change in the mechanism controlling the gasification rate, with chemical reaction rates controlling it at temperatures below 530 °C and desorption rates controlling it at temperatures above 530 °C.

As for A&B's $k_G^g(T_{hold}, 11\text{ atm})$ versus ${T_{hold}}^{-1}$ plot, $k_G^g(T_{hold}, 11\text{ atm})$ values were lower than $k_G^g(T_{hold}, 2\text{ atm})$ values for T_{hold} values greater than 500 °C. But there was no break in the plot's slope, and $k_G^g(T_{hold}, 11\text{ atm})$ values were higher than $k_G^g(T_{hold}, 2\text{ atm})$ values for T_{hold} values less than 500 °C.

The latter result was surprising to us. While we could imagine that, impeded by a denser gas, desorption rates into 11-atm Ar would be lower than those into 2-atm Ar, we could not imagine that the difference in pressure would have any impact on the rates of the condensed-phase's chemical reactions. Therefore, we could not imagine how gasification rates into 11-atm Ar could be greater than those into 2-atm Ar at any given temperature.

Toward establishing the model's capacity to reproduce A&B's findings, we ran a series of simulations in which the species desorption rates were varied by heuristically varying $\alpha_j k_j^d$. To start, we set all k_j^d values equal to a constant (A^d); α_j equal to 0 for the five species in the mechanism (including EODT) with molecular weights 271 amu and higher* and all other α_j equal to 1. We also set P_{HFV} equal to 1. The cumulative mass of gasified products generated by a given time [$m_g(t)$] was equal to $m_0 - m_c(t)$.

Representative results for the low and high ends of the T_{hold} range of A&B's study are shown in Fig. 4. In general, the trends in the calculated gasification rates were as (we) expected, increasing to start then declining as m_c declined. Except (perhaps) for rates produced with A^d set equal to 0.1 s^{-1}, there were no 0.5- to 2-s intervals bounding maximum rates that were "steady" and thus construable as a zeroth-order kinetic process. In addition, at the low end of the T_{hold} range, of which the T_{hold} = 480 °C results shown in Fig. 4 are representative, the time for more than 95% of m_0 to gasify was far longer than the durations of A&B's experiments (19 s). In all simulations in which $A^d \geq 1.0$ s^{-1}, the maximum gasification rate occurred within 19 s. However, in Fig. 2 of A&B-II (A&B 1996b) the process appears to have completed in less than 10 s, and thus indicated a gasification rate that was far higher than those predicted by the HR model even though reactions rates were as high as producible with the chemical kinetics mechanism ($P_{HFV} = 1$).

*Following from our expectation that C-C bonds in R45M must break for gasifiable products to form, this prescription imposed an analogous constraint; only products generated via a path involving the breaking of at least one of EODT's C-C bonds were gasifiable.

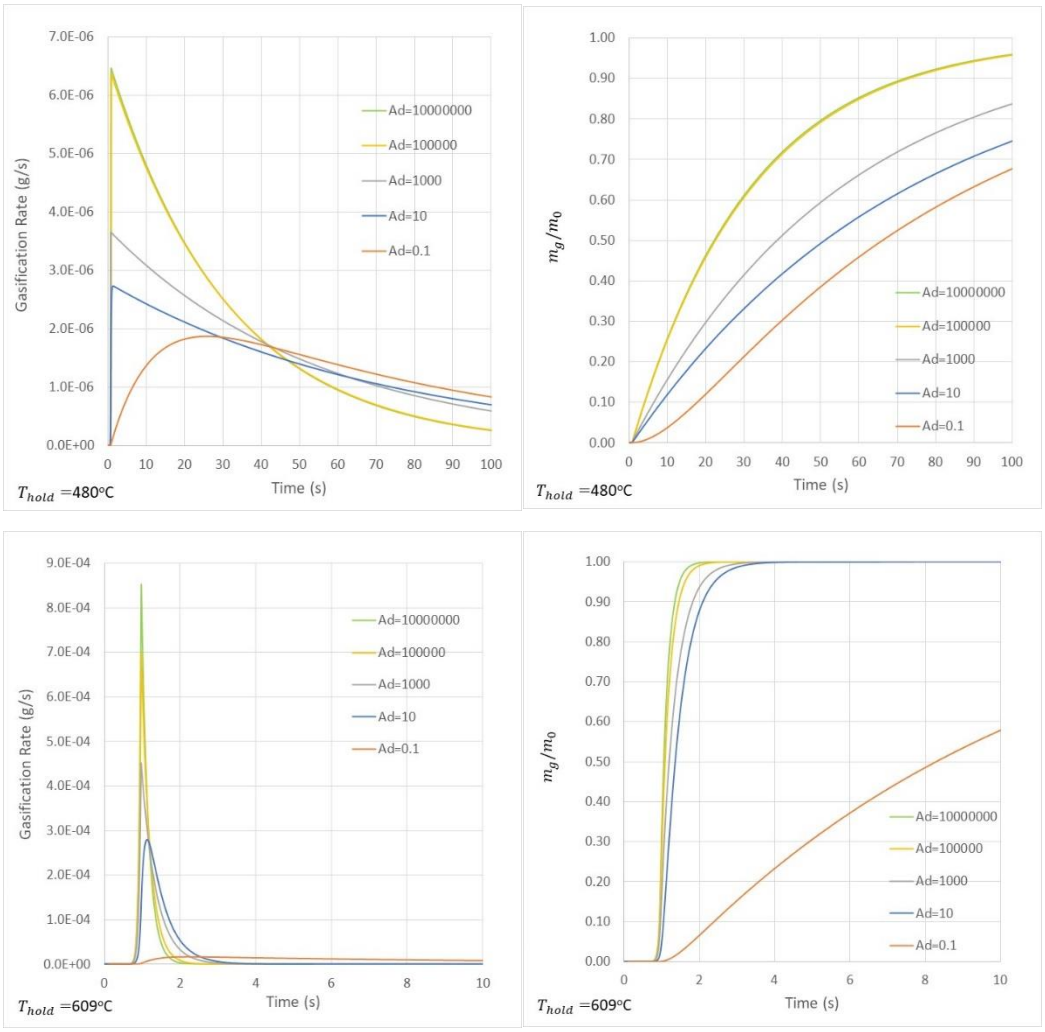

Fig. 4 Representative examples of HR-model-generated dm_c/dt and m_g/m_0 vs. t data as a function of A^d (in s^{-1})

As discussed in Section 2.2, the $k_G^g(T_{hold}, P)$ values A&B derived per Eq. 2 corresponded to maximum gasification rates. Therefore, to compare the model-predicted gasification rates to the $k_G^g(T_{hold}, P)$ values A&B reported, we divided the maximum computed gasification rate $\left(r_G^{g,max}\right)$ at a given T_{hold} and A^d by m_0 (200 μg). The results are presented in Fig. 5. As shown, the break in the slope of the measurement-based $k_G^g(T_{hold}, 2\,\text{atm})$ versus ${T_{hold}}^{-1}$ plot was only clearly present in the series of simulations produced with A^d equal to 0.1 or 1.0 s^{-1}. However, in these two cases, the differences between measurement-derived and model-predicted values were over a factor of two at low end of the T_{hold} range and became larger as T_{hold} increased.

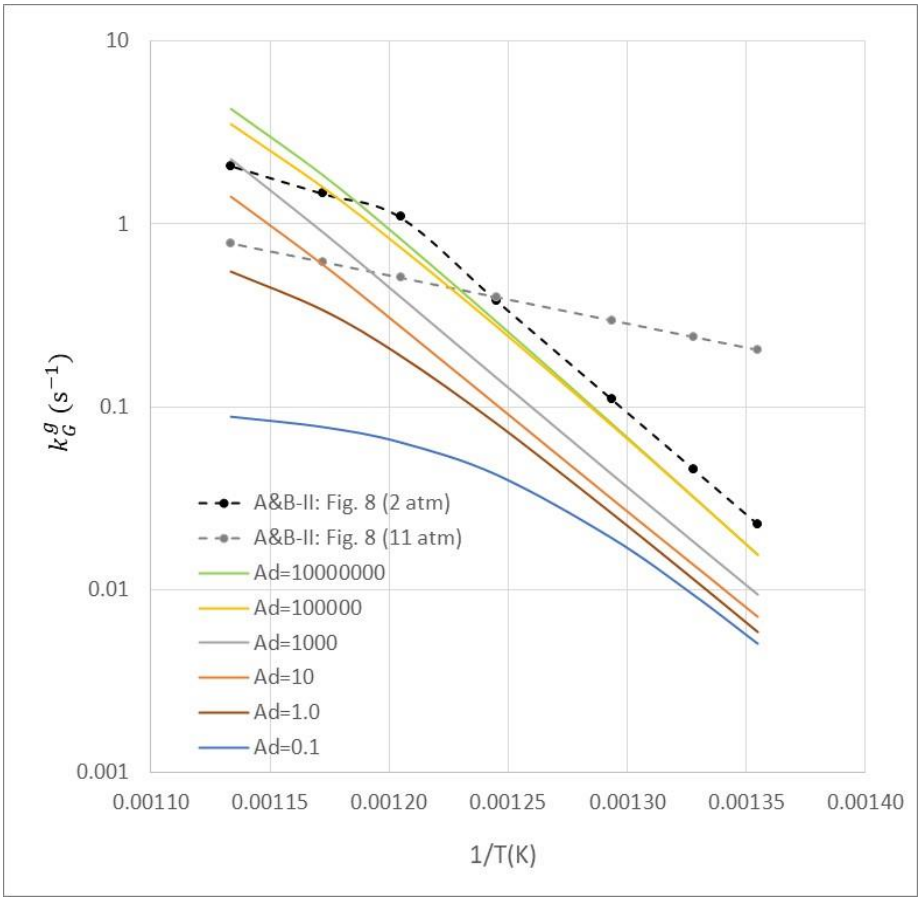

Fig. 5 Comparisons of HR model-based and measurement-derived $k_G^g(T)$ values

For series produced with higher A^d values, the $k_G^g(T_{hold})$ predictions asymptotically approached A&B's $k_G^g(T_{hold}, 2\text{ atm})$ values. And consistent with our expectation that $k_G^g(T_{hold}, 2\text{ atm})$ would be greater than $k_G^g(T_{hold}, 11\text{ atm})$ for all T_{hold}, the $k_G^g(T_{hold})$ versus ${T_{hold}}^{-1}$ plots for different A^d never crossed. Indeed, rather than the (effective) k_G^d value simply representing a limit for $k_G^g(T_{hold})$ (as suggested by A&B's interpretation of their data), our model produced maximum gasification rates that were below the limit supportable by chemical kinetics rates even though the limit represented by the desorption rate was far higher, demonstrating the coupling between the two processes.

4.2 Final Gas-Phase Product Mass Fractions

Figure 6 shows the gas-phase products to which A&B attributed features of the spectra generated by their FTIR probe. A&B stated that at the end of the experiments the (gas-phase) mass of these species (plus cis- and vinyl-butadiene oligomers that are not shown) equaled approximately 70 wt% of the sample's initial mass, and that 95–98 wt% of all gas-phase products comprised 1,3-butadiene,

4-vinyl-cyclohexene, ethylene, 1,5-hexadiene, cyclopentene, and trans-butadiene oligomers. Our mechanism did not include 1,5-hexadiene or dimethylether (DME). (Reactions involving DME were in the full EODT–RFNA–air mechanism but they were stripped from it in creating the mechanism employed for the simulations because DME had an oxygen atom and therefore had no potential to be produced by a starting chemical composition comprising only EODT.) With respect to its capacity to represent trans-, cis-, or vinyl-butadiene oligomers that A&B labeled *t*-BDO, *c*-BDO, and *v*-BDO, respectively, the mechanism had 150 species (besides EODT, 4-vinyl-cyclohexene [VYC6E3], and the four species for whom α_j was set equal to 0) with eight or more carbon atoms. However, believing that most oligomers would (like nominal R45M polymer chains) comprise combinations of trans, cis, and vinyl butadiene monomers, we doubted A&B's distinctions were warranted and therefore that it was necessary to assign these species to one of the three types. Rather, we simply classified all such species as *t*-BDO and summed their Y_j^∞s to assess whether the model produced mass fractions for high-molecular-weight molecules comparable to those reported by A&B for *t*-BDO.

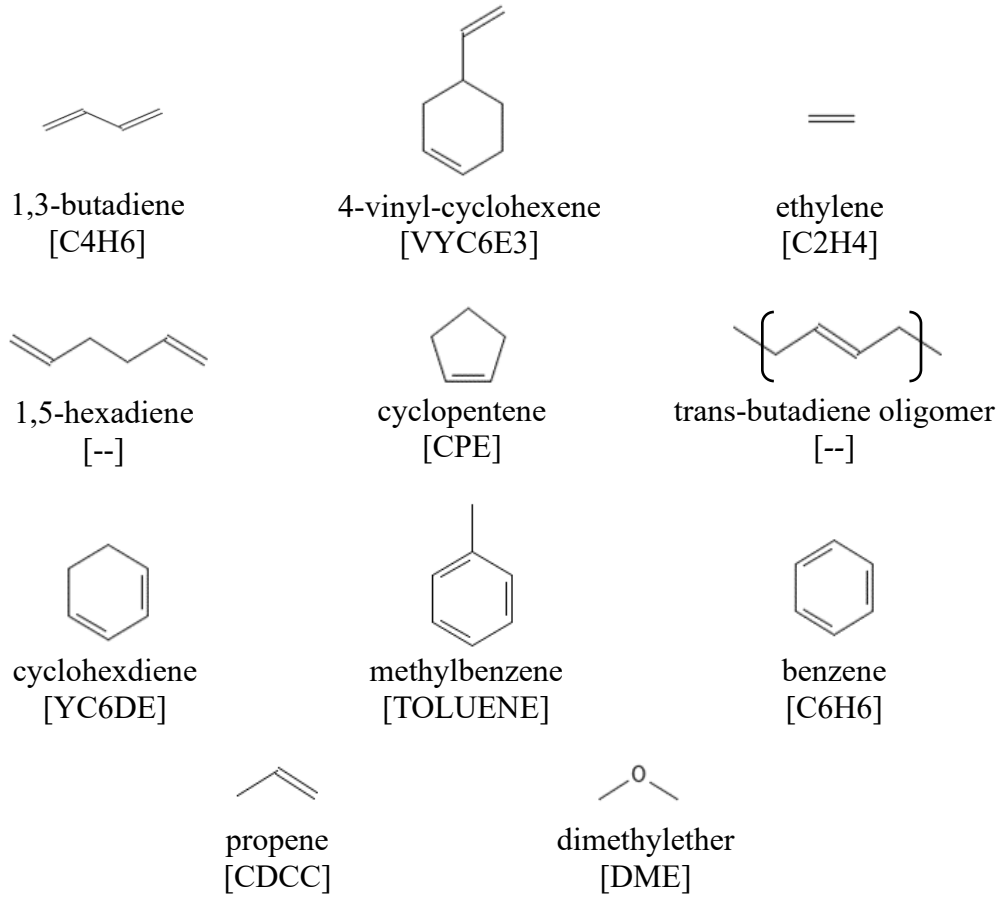

Fig. 6 Major and minor species detected in A&B's T-jump experiments. Bracketed names are the species' labels in the mechanism.

Tables 1 and 2 show for simulations having T_{hold} values equal to 480 and 609 °C, respectively, $Y_j^{\infty}(A^d)$ predictions for all the species in the mechanism that in at least one of the simulations analyzed for this study had a Y_j^{∞} greater than 0.005. There were 46 in all. The eight molecules with well-defined molecular structures that A&B observed and were in the chemical kinetics mechanism met this criterion. We also note that, as was to be expected, the lower gasification rates produced by lower A^d values led to longer times for chemical reactions to occur, and that resulted in higher Y_j^{∞} for small molecules. (Compare results produced with A^d = 0.1 s^{-1} to those produced with A^d = 10,000,000 s^{-1}.)

Figure 7 presents model-predicted $Y_j^{\infty}(T_{hold}, A^d)$ values for five of the six major products observed by A&B and compares them to their measurement-based counterparts. All-in-all, the comparisons did not raise any particular concerns about the chemical kinetics mechanism's validity or its potential value for understanding R45M's pyrolysis. Indeed, except for the Y_{CPE}^{∞} predictions, the predictions produced with A^d = 1.0 s^{-1} were highly encouraging. The results produced with $A^d \geq$ 100,000 s^{-1} suggested those values were too high. For $A^d \leq$ 10,000 s^{-1}, the $\sum Y_{C_{n\geq 8}H_m}^{\infty}$ predictions we took to represent Y_{t-BDO}^{∞} were low relative to measured values but encouragingly had magnitudes larger than Y_{C4H6}^{∞}. Similarly, the magnitudes of the predictions for Y_{C2H4}^{∞} and Y_{CPE}^{∞} relative to those for Y_{C4H6}^{∞} were consistent with the measured values.

Table 1 Species whose Y^{∞} exceeded 0.005 in at least one simulation: T_{hold} = 480 °C[a,b]

					A^d (s^{-1})				
	Label	**MW**	**C**	**H**	**1E-1**	**1E1**	**1E3**	**1E5**	**1E7**
2	CH4	16.04	1	4	8.6E-03	7.9E-03	–	–	–
3	**C2H4**	28.05	2	4	6.8E-03	–	–	–	–
4	C2H6	30.07	2	6	8.3E-03	5.9E-03	–	–	–
5	**CDCC**	42.08	3	6	1.0E-02	1.0E-02	–	–	–
6	C3H8	44.10	3	8	–	–	–	–	–
7	**C4H6**	54.09	4	6	5.3E-02	2.1E-01	2.2E-01	2.8E-02	–
8	C4H71-3	55.10	4	7	–	1.1E-01	1.9E-01	6.5E-02	4.7E-02
9	C4H8-1	56.11	4	8	7.6E-02	5.2E-02	3.0E-02	1.7E-02	1.7E-02
10	C4H8-2	56.11	4	8	–	–	–	–	–
11	C4H10	58.12	4	10	–	–	–	–	–
12	CVV	68.12	5	8	5.6E-02	4.6E-02	3.2E-02	–	–
13	**CPE**	68.12	5	8	–	–	–	–	–
14	C5H10-2	70.14	5	10	–	–	–	–	–
15	**C6H6**	78.11	6	6	–	–	–	–	–
16	**YC6DE**	80.13	6	8	–	–	–	–	–
17	VVV	80.13	6	8	1.8E-02	1.6E-02	–	–	–
18	CCPDE	80.13	6	8	9.9E-03	8.3E-03	–	–	–
19	**TOLUENE**	92.14	7	8	–	–	–	–	–
20	CHDEM	94.16	7	10	3.3E-02	3.3E-02	1.6E-02	–	–
21	VCPE	94.16	7	10	1.2E-02	6.6E-03	–	–	–
22	CCCPDE	94.16	7	10	–	–	–	–	–
23	STYRENE	104.15	8	8	–	–	–	–	–
24	VY6DE13	106.17	8	10	–	–	–	–	–
25	C6H5CC	106.17	8	10	–	–	–	–	–
26	**VYC6E3**	108.18	8	12	1.5E-01	8.1E-02	9.4E-02	1.1E-02	–
27	CVCVV	108.18	8	12	1.1E-01	8.7E-02	4.6E-02	7.7E-03	5.9E-03
28	CVCVIV	108.18	8	12	2.8E-02	1.8E-02	1.6E-02	–	–
29	CVCZCVCJ	109.19	8	13	–	3.9E-04	2.0E-02	2.0E-01	2.6E-01
30	CCJYC6E3	109.19	8	13	–	–	7.9E-03	1.4E-02	–
31	CCJYCCVCM	109.19	8	13	–	–	–	1.1E-02	–
32	CJVCMVC	109.19	8	13	–	–	2.7E-02	2.9E-02	–
33	CCVCJVC	109.19	8	13	–	6.6E-03	2.0E-02	–	–
34	CCCVVCJ	109.19	8	13	–	5.2E-03	5.8E-03	–	–
35	IND	116.16	9	8	–	–	–	–	–
36	CVCCVV	122.21	9	14	–	–	–	–	–
37	NAPH	128.18	10	8	–	–	–	–	–
38	BBVV	162.28	12	18	6.5E-03	–	–	–	–
39	CJVCGB	163.29	12	19	–	–	8.6E-03	1.1E-01	1.3E-01
40	BZBBJ	163.29	12	19	–	–	1.3E-02	2.2E-01	2.6E-01
41	VCCGB	164.29	12	20	–	3.6E-02	1.9E-02	9.1E-03	8.9E-03
42	BZBB	164.29	12	20	3.9E-02	–	–	–	–
43	BBBCJV	203.35	15	23	–	–	–	–	–
44	BZBBVC	204.36	15	24	1.4E-01	9.2E-02	7.5E-02	1.2E-02	1.2E-02
45	BZBBVIV	216.37	16	24	1.7E-01	1.5E-01	1.2E-01	6.7E-02	6.6E-02
46	BCCIVBZBJ	217.38	16	25	–	–	8.9E-03	1.6E-01	1.7E-01
47	BBBCIVCJ	217.38	16	25	–	–	–	–	9.6E-03
	$\sum Y(C_{n\geq 8}H_m)$[c]				5.4E-01	4.1E-01	4.0E-01	8.7E-01	9.3E-01

[a] Species with bold labels were observed by A&B. [b] To help visualize the trends in the data, only values ≥0.005 are shown. [c] The sum does not include the Y^{∞} for VYC6E3.

Table 2 Species whose Y^{∞} exceeded 0.005 in at least one simulation: T_{hold} = 609 °C[a,b]

					A^d (s^{-1})				
	Label	**MW**	**C**	**H**	**1E-1**	**1E1**	**1E3**	**1E5**	**1E7**
2	CH4	16.04	1	4	7.6E-02	1.1E-02	–	–	–
3	**C2H4**	28.05	2	4	7.5E-03	7.7E-03	–	–	–
4	C2H6	30.07	2	6	2.2E-02	9.7E-03	–	–	–
5	**CDCC**	42.08	3	6	2.1E-02	1.3E-02	8.3E-03	–	–
6	C3H8	44.10	3	8	2.3E-02	–	–	–	–
7	**C4H6**	54.09	4	6	4.0E-02	1.7E-01	3.4E-01	1.6E-01	–
8	C4H71-3	55.10	4	7	–	–	2.0E-01	1.6E-01	5.7E-02
9	C4H8-1	56.11	4	8	3.6E-02	5.5E-02	2.6E-02	1.2E-02	9.3E-03
10	C4H8-2	56.11	4	8	1.9E-02	1.4E-02	8.8E-04	–	–
11	C4H10	58.12	4	10	1.3E-02	–	–	–	–
12	CVV	68.12	5	8	1.3E-02	3.3E-02	2.5E-02	6.8E-03	–
13	**CPE**	68.12	5	8	1.2E-02	–	–	–	–
14	C5H10-2	70.14	5	10	1.2E-02	–	–	–	–
15	**C6H6**	78.11	6	6	5.7E-02	–	–	–	–
16	**YC6DE**	80.13	6	8	3.0E-02	6.8E-03	5.1E-03	–	–
17	VVV	80.13	6	8	1.7E-02	3.1E-02	1.4E-02	–	–
18	CCPDE	80.13	6	8	6.3E-03	–	–	–	–
19	**TOLUENE**	92.14	7	8	1.7E-01	1.3E-02	–	–	–
20	CHDEM	94.16	7	10	1.3E-03	2.2E-02	1.6E-02	–	–
21	VCPE	94.16	7	10	1.0E-02	1.1E-02	–	–	–
22	CCCPDE	94.16	7	10	–	–	–	–	–
23	STYRENE	104.15	8	8	1.1E-01	–	–	–	–
24	VY6DE13	106.17	8	10	–	–	–	–	–
25	C6H5CC	106.17	8	10	2.6E-02	–	–	–	–
26	**VYC6E3**	108.18	8	12	2.8E-02	6.9E-02	4.4E-02	3.2E-02	–
27	CVCVV	108.18	8	12	6.1E-03	1.6E-01	9.7E-02	3.1E-02	3.8E-03
28	CVCVIV	108.18	8	12	6.1E-02	3.3E-02	1.8E-02	9.0E-03	–
29	CVCZCVCJ	109.19	8	13	–	–	–	1.1E-01	2.5E-01
30	CCJYC6E3	109.19	8	13	–	–	–	1.2E-02	1.2E-03
31	CCJYCCVCM	109.19	8	13	–	–	–	5.7E-03	–
32	CJVCMVC	109.19	8	13	–	–	–	5.1E-02	–
33	CCVCJVC	109.19	8	13	–	–	9.1E-03	1.1E-02	–
34	CCCVVCJ	109.19	8	13	–	–	7.1E-03	–	–
35	IND	116.16	9	8	2.3E-02	–	–	–	–
36	CVCCVV	122.21	9	14	–	7.1E-03	–	–	–
37	NAPH	128.18	10	8	1.7E-02	–	–	–	–
38	BBVV	162.28	12	18	–	2.4E-02	5.6E-03	–	–
39	CJVCGB	163.29	12	19	–	–	–	6.1E-02	1.4E-01
40	BZBBJ	163.29	12	19	–	–	–	1.0E-01	2.4E-01
41	VCCGB	164.29	12	20	1.4E-02	5.2E-02	2.7E-02	6.6E-03	5.1E-03
42	BZBB	164.29	12	20	3.9E-02	7.4E-02	–	–	–
43	BBBCJV	203.35	15	23	–	–	–	1.3E-02	1.1E-02
44	BZBBVC	204.36	15	24	2.1E-02	6.2E-02	3.8E-02	1.5E-02	7.3E-03
45	BZBBVIV	216.37	16	24	1.1E-02	9.1E-02	7.6E-02	4.5E-02	3.6E-02
46	BCCIVBZBJ	217.38	16	25	–	–	–	1.2E-01	1.9E-01
47	BBBCIVCJ	217.38	16	25	–	–	–	–	2.1E-02
	$\sum Y(C_{n\geq 8}H_m)$[c]				3.7E-01	5.1E-01	2.9E-01	6.2E-01	9.2E-01

[a] Species with bold labels were observed by A&B. [b] To help visualize the trends in the data, only values ≥0.005 are shown. [c] The sum does not include the Y^{∞} for VYC6E3.

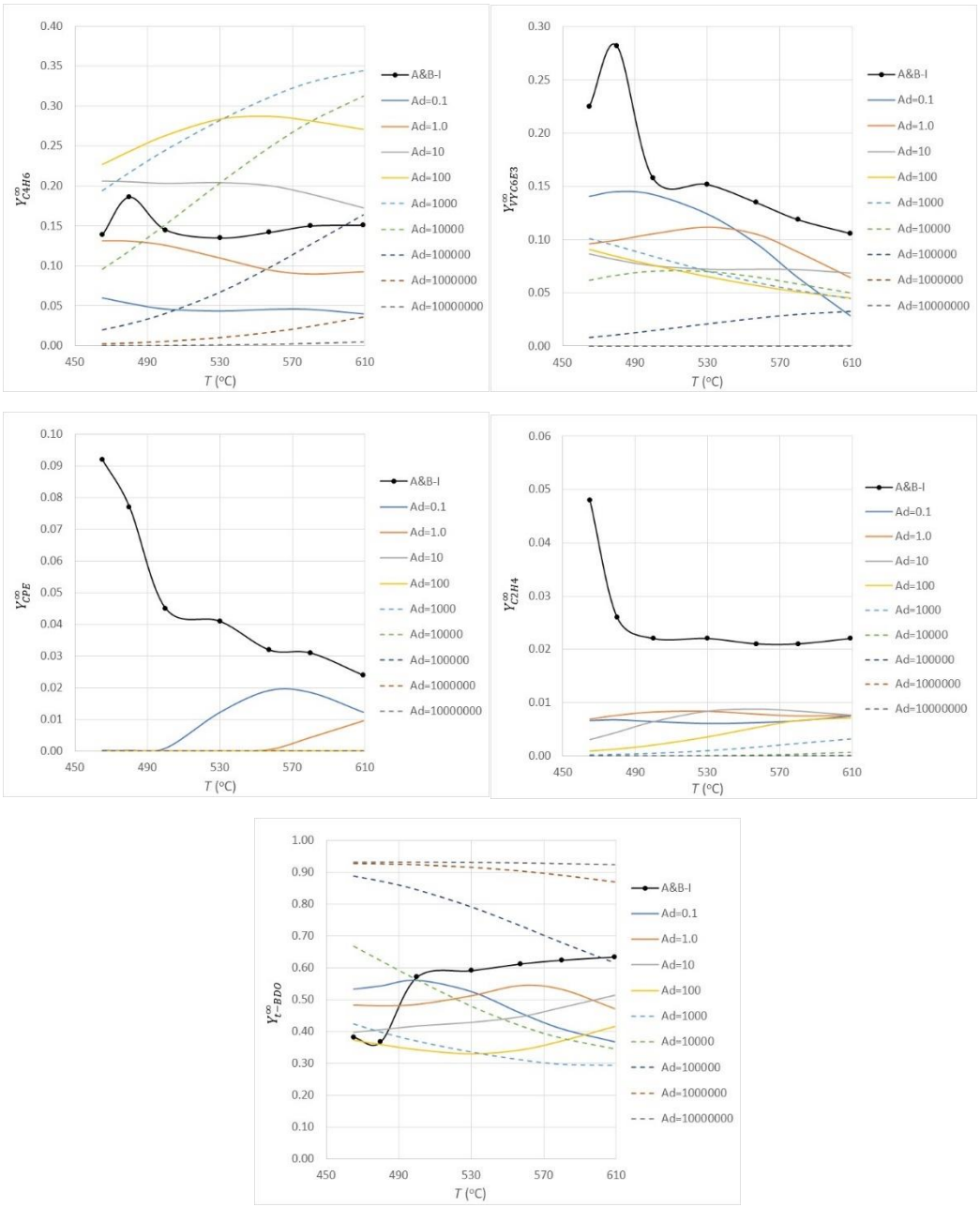

Fig. 7 Comparison of measured and predicted Y_j^{∞} as a function of T_{hold} and A^d (in s^{-1})

4.3 1,3-Butadiene (C4H6) Gasification Rates

Figure 8 compares measured and predicted $C_{C4H6}(480\ ^{o}C, t)$ values for the nine A^d values that were specified in the study. As discussed in Section 2.2, the conversion of model-predicted gasification rates into $C_{C4H6}(T_{hold}, t)$ estimates assumed that V was 25 cm^3. That specification produced $C^{\infty}_{C4H6}(480\ ^{o}C)$ predictions that were in reasonable agreement with the measured value for $10 \leq A^d \leq 1000$. However, the time required for $C_{C4H6}(t)$ to approach C^{∞}_{C4H6} was over a factor of 10 longer.

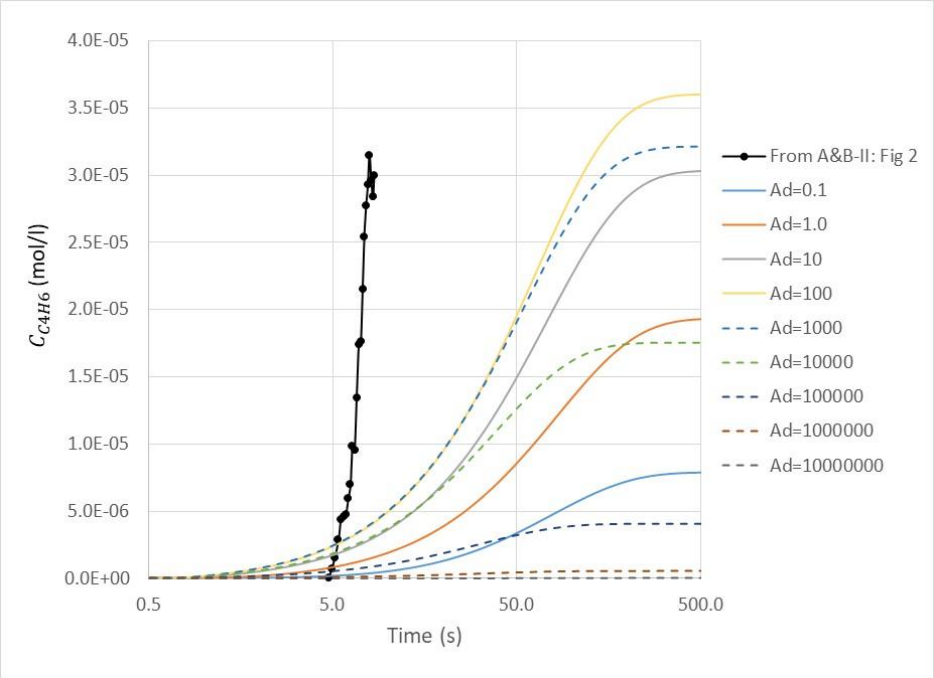

Fig. 8 Comparison of measured and predicted C_{C4H6} (t) values (A^d in s^{-1})

As noted in Section 2.2, V was not reported. The 25-cm^3 value was reported in a previously published study (Brill 1994). However, based on data reported in A&B-I/II (1996a,b), we obtained an estimate suggesting it was closer to 3.3 cm^3. The use of that value for computing $C_{C4H6}(t)$ of course produced values that were nearly eight times greater than those presented in Fig. 8, yielding better agreement between the measured C^{∞}_{C4H6} value and predictions produced with some A^d values and worse agreement in other cases. While there was some temptation to compare other features of the simulations to the measurement-based results to establish the A^d value that best represented the process, by that point we had come to suspect that the discrepancies between the predicted and measured gasification rates were due to bubble-promulgated mass transfer playing an important role in the gasification process and not being represented in the model. The possibility that rate-accelerating catalysis effected by the Pt filament had also occurred to us. Thus, we did not believe further exploration of the differences between measured and predicted $C_j(t)$ values was warranted.

Underlying our suspicion that mass transfer from the condensed phase to the gas phase in the experiments was not solely due to desorption/evaporation from a mechanically quiescent free surface was our previous experience in modeling such scenarios. For example, we have successfully represented evaporative mass fluxes ($\dot{m}_{c\rightarrow g}$) using an HLK relationship,

$$\dot{m}_{c\to g} = \sum_j \alpha_j \left(\frac{W_j}{2\pi R T^0}\right)^{\frac{1}{2}} \left(X_{c\to g,j} P_{eq,j}(T^0) - X_j^{0+} P\right), \qquad (10)$$

where $X_{c\to g,j}$ is the gasifying substance's mole fraction at the surface, X_j^{0+} is its mole fraction in the gas phase adjacent to the surface, and $P_{eq}(T)$ is its equilibrium vapor pressure, which we represented with

$$P_{eq}(T^0) = A' exp\left(-\frac{B'}{T^0}\right) \qquad (11)$$

where *A'* and *B'* are constants.

To get a sense for how long it would take to simply evaporate a 200-μg sample of EODT that was 100 μm thick (and thus had a surface area of approximately 1 cm^2), we noted that the measured normal boiling point of *n*-icosane ($C_{20}H_{42}$) (i.e., T_b where $P_{eq}(T_b)$ = 1 atm) is 343 °C (Weast and Grasselli 1989). Group additivity-based estimates for it and EODT were, respectively, 334 and 341 °C (Stein and Brown 1994). Taken together, they indicated 1) the group additivity method was reasonably reliable, and 2) the boiling points of *n*-icosane and EODT were similar. Substituting property values for EODT into Eq. 10 and assuming $X_j^{0+}P$ could be neglected yielded an $\dot{m}_{c\to g}$ equal to 9 g/cm^2-s. This suggested that the sample would completely evaporate in less than 3×10^{-5} s, a value that was miniscule compared to the time scale of the dynamics observed by A&B. And, of course, the value would have been even smaller in the range of T_{hold} values at which the experiments were conducted. Thus, it was difficult for us to imagine that the gasification of a chemical composition comprising hydrocarbons with molecular weights similar to or less than EODT's could be desorption limited. As noted long ago by Zeldovich (1942), it is extremely difficult to superheat a material with a free surface (because the gasification rates are so high). Rather, we thought it likely that in the experiments the pyrolysis products adjacent to the filament boiled but, being trapped by the colder, less decomposed layer above them, created a bubble field that eventually burst through the surface, producing the sharp increases in C_j that A&B observed.

Consistent with our hypothesis, A&B noted that the residue on the filament they observed following experiments in the range 465–500 °C appeared white due to the inclusion of bubbles. Among other things, differences in bubble formation might explain the difference in A&B's and Ericsson's (1978) findings. We would guess that bubble formation would be less prominent in the 7-μg samples pyrolyzed by Ericsson than the 200-μg samples pyrolyzed by A&B. In addition, differences in bubble formation and release could be the reason measurement-based $k_G^g(T, 11\ \text{atm})$ values were greater than their $k_G^g(T, 2\ \text{atm})$ counterparts for T_{hold} < 500 °C. We imagine that when the pressure in the cell was 11 atm, which

compared to 2 atm would not only present a higher barrier to desorption but also a greater heat sink that would retard decomposition at the surface, the gaseous pyrolysis products would be trapped longer, forming smaller products that would release more quickly once the surface broke. Had A&B published the time at which products were first detected at each T_{hold} and P, our hypothesis might have been corroborated.

Suspecting that bubble-promulgated mass transport was important, we could (perhaps) have attempted to add to Eq. 6 a source term to represent such a process. However, from the standpoint of achieving the two main objectives of this study, namely corroboration for the validities of 1) our framework for modeling the deflagration of R45M in either an OFDF experiment or a SFRJ combustor, and 2) our framework for modeling condensed phase reaction chemistry, we thought there would be little benefit. In the T-jump experiments the temperature gradient within the sample (along a path from the filament to the interface between the condensed and gas phases) was negative, while the density gradient along that path was positive. As such, that combination has the potential to promote bubble formation. In a deflagrating material the temperature gradient along the analogous path is positive, while the density gradient is negative, and therefore bubbling would (presumably) be less likely.

4.4 Exothermicity?

As mentioned in Section 2.1, A&B measured the difference between the voltage required to heat the sample–filament system and that needed to heat the filament alone to obtain an indication of whether the pyrolysis process was releasing or absorbing heat. In the one plot of such data that A&B provided (see Fig. 13 of A&B-I [1996a]), the process was endothermic during the first 3 s, then exothermic for about 4 s, by which point it had asymptotically approached thermoneutral.

Bouck et al. (1973) also observed R45M's pyrolysis at high heating rates to be exothermic. Nonetheless, we were skeptical. For systems containing very little oxygen, that result essentially requires that the (endothermic) breaking of single bonds in acyclic hydrocarbon chains be more than offset by the (exothermic) creation of ring-forming single bonds. Given the results published by Ganesh (2000), we could not completely ignore the possibility. But given the overall decline in the number of atoms in the products, it seemed implausible. In addition, it takes energy to volatilize a substance. For example, the enthalpy of vaporization of *n*-icosane at 267 °C is approximately 17 kcal/mol (Chirico et al. 1989). Relative to the potential for the oxidizer-free pyrolysis of a hydrocarbon to be (chemically) exothermic, that value is not insignificant.

To determine if the model produced processes that at any point were exothermic, we checked the $\dot{q}$ versus t tables generated by Eq. 9 for each simulation. The only (A^d, T_{hold}) cases that yielded $\dot{q} > 0$ were $(A^d = 0.1\ \mathrm{s}^{-1}, T_{hold} \geq 530\ ^{\mathrm{o}}\mathrm{C})$ and $(A^d = 1.0\ \mathrm{s}^{-1}, T_{hold} \geq 580\ ^{\mathrm{o}}\mathrm{C})$. Figure 9 shows $\dot{q} * m_c$ versus t plots that are representative of the remainder. In short, consistent with our expectations, the reaction chemistry was endothermic over the entire duration of the simulations. Including the heat needed to volatilize the products would have made the processes more so.

Given that $\dot{q}$ results consistent with our expectations were produced by simulations that generated $k_G^g(T)$ predictions in better agreement with A&B's measurement-based values than those that were not, we likely would have dismissed those that were not out of hand had other results not led us to suspect that a bubble field trapped close to the filament was created in the experiments. To the extent we imagine that desorption *would* be limited in such a scenario (albeit in a manner different than our model's representation of the process), the $\dot{q} > 0$ results produced by the $(A^d = 0.1\ \mathrm{s}^{-1}, T_{hold} \geq 530\ ^{\mathrm{o}}\mathrm{C})$ and $(A^d = 1.0\ \mathrm{s}^{-1}, T_{hold} \geq 580\ ^{\mathrm{o}}\mathrm{C})$ simulations suggest the reaction chemistry in a bubble field trapped close to the filament might in fact have the potential to be exothermic. Additionally, we note that A&B's samples comprised polymer chains that were terminated by -OH groups. Therefore, they had more potential to promulgate exothermic reactions than our (idealized) construct, which contained no O atoms. Evidence supporting this possibility is A&B's observation of DME. In addition, in the IR spectra presented in Fig. 5 of A&B-I, there is a prominent feature near 2000 cm^{-1} that is not discussed. (We do not know why.) We believe it could be attributable to CO. Thus, we consider it possible that pyrolysis products reacting with O_2 adsorbed by the samples might also have contributed to the exothermicity A&B detected. We also consider it possible that catalysis of the process by the Pt filament might have contributed to the result.

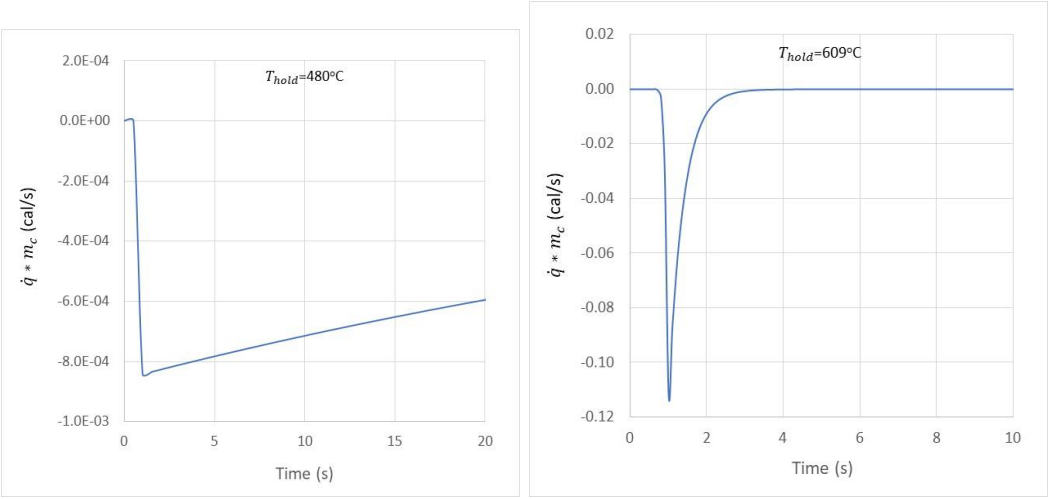

Fig. 9 $\dot{q} * m_c$ **vs.** t **plots:** $A^d = 1000\ s^{-1}$

5. R45M'S Pyrolysis in Opposed Flow Diffusion Flame Experiments

At the start of this study, we believed A&B's findings would be a good basis for validating the EODT pyrolysis (sub)mechanism because we thought the conditions A&B established in their T-jump experiments would approximate those that would be generated in an OFDF experiment or an SFRJ's combustor. However, as discussed in Section 4.3, the juxtaposition of the temperature and density gradients produced in the T-jump experiments was different than that in the applications of interest, limiting the value of the experiments' results for mechanism-model validation. Nonetheless, the effort motivated us to estimate the temperature transients to which a subsurface layer of R45M would be subject in OFDF experiments prior to reaching the burning surface, then employ them as a basis for estimating the extent to which the layer would pyrolyze just prior to gasifying.

The temperature transients to which a layer within a sample burning at a constant rate (u) would be subject prior to reaching the surface were estimated via a previously employed approach (McQuaid et al. 2015). Presuming the condensed-phase's density (ρ_c), heat capacity (c_p), and thermal conductivity (λ) can be reasonably represented with temperature-independent constants, the energy equation in a spatial coordinate system (x) that moves at u relative to a space-fixed system reduces to

$$\frac{d^2T(x)}{dx^2} + \frac{\rho u c_p}{\lambda}\frac{dT(x)}{dx} = 0. \qquad (12)$$

With appropriate/standard boundary conditions, the solution to Eq. 12 is

$$T(x) = T^{\infty} + (T^{0} - T^{\infty})exp\left[-\frac{\rho u c_p}{\lambda}x\right] \quad (13)$$

where T^{∞} is the initial (bulk) temperature of the condensed phase and T^{0} is the temperature at the surface (x = 0). It then follows that for a layer that is a distance (d^{0}) from the burning surface at t = 0,

$$T(d^{0}, t) = T^{\infty} + (T^{0} - T^{\infty})exp\left[-\frac{\rho u c_p}{\lambda}(d^{0} - ut)\right]. \quad (14)$$

Produced with the input parameters shown in Table 3, Fig. 10 presents plots of T as a function of x and t for T^{0} = 477 °C (750 K) and u = 0.005, 0.01, or 0.02 cm/s. The u values cover a range of burning rates that our collaborators have reported (Geipel et al. 2022). While we are unaware of any measurements to which these transients could be compared, their time and length scales appeared reasonable to us.

Table 3 Property values employed to estimate the temperature transient to which a subsurface layer in a deflagrating HTPB/R45M strand will be subject prior to reaching the surface

Property	Units	Value
λ	W/m-K-s	0.5
ρ	g/cm^3	0.9
c_p	J/g-K	2.0

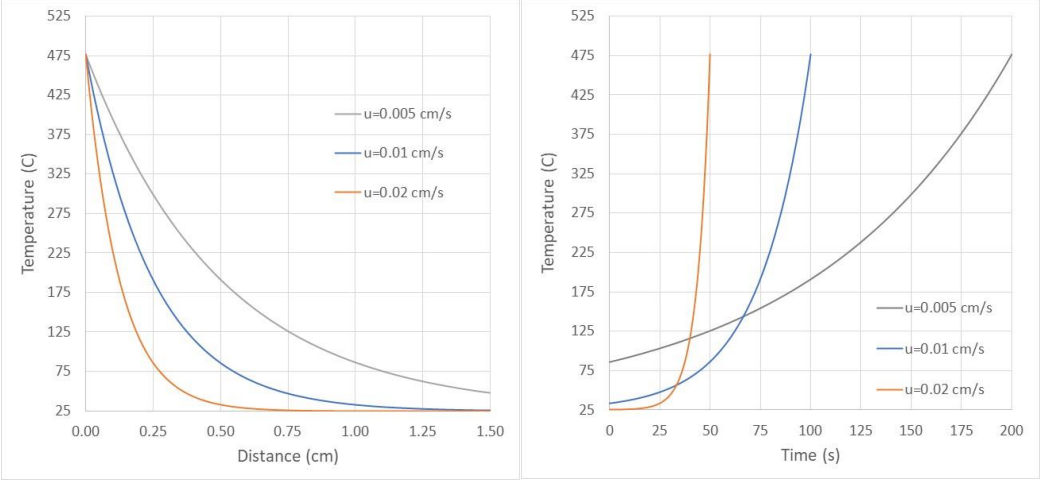

Fig. 10 Estimates for the temperature transients in R45M samples deflagrating in OFDF experiments as a function of the burning rate: a) spatial profiles, and b) temporal profiles in a layer that is 1 cm from the surface at t = 0

To model the evolution of the species concentrations in a layer subject to these transients, we employed the solutions to specify the temperature of a system represented by Eq. 7 with α_j = 0 for all j. Results for Y_{EODT} are presented in Fig. 11.

As was expected, the final Y_{EODT} values were inversely proportional to the burning rate. But even at the lowest rate (0.005 cm/s), less than 15% of the initial mass of EODT in the layer was decomposed by the time it had reached the surface. Moreover, that result was obtained with P_{HFV} = 1, and thus corresponded to chemical reaction rates that will likely exceed those in actual systems. As such, these findings increased our confidence that for modeling the deflagration of R45M in OFDF experiments, EODT is far more representative of the nascent gas-phase products of the pyrolysis process than a light hydrocarbon such as C2H4 or C4H6.

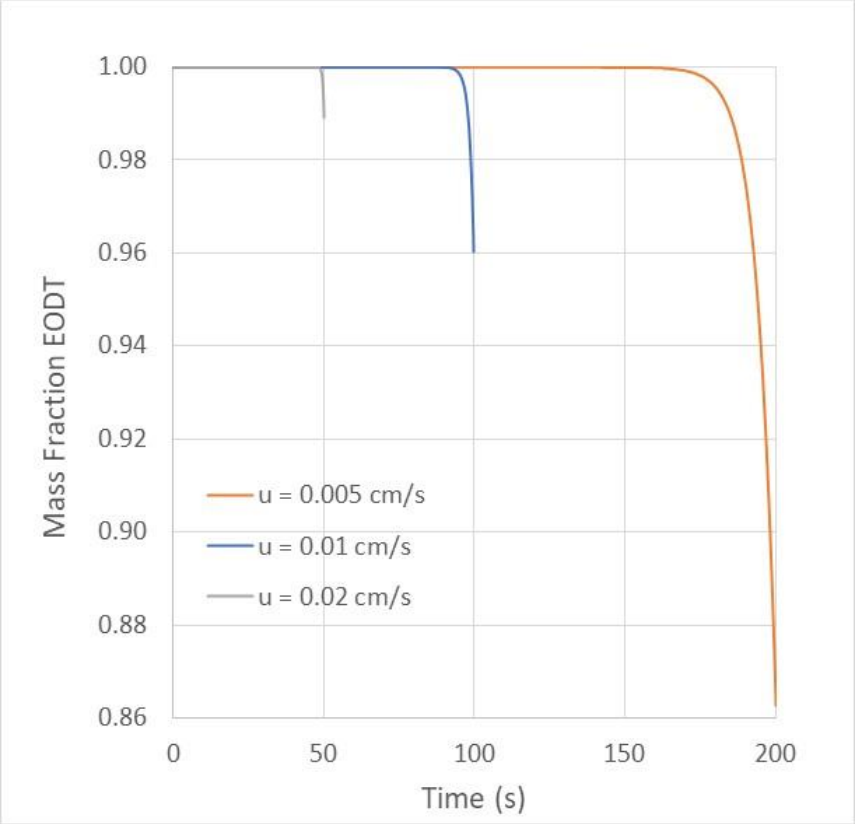

Fig. 11 Estimates for $Y_{EODT}(t)$ in a subsurface layer up to the point it reaches the surface as a function burning rate

6. Summary and Conclusions

Seeking to validate a paradigm for modeling the deflagration of R45M that is predicated on the nascent gas-phase products of its pyrolysis being represented by EODT, we formulated and applied a model for simulating EODT's pyrolysis and product gasification when subject to conditions established by A&B in T-jump experiments. Finding that the model's predictions for the time necessary for the process to go to completion at the low end of the T_{hold} range of the experiments was considerably longer than the experiments' 19-s (max) duration, we concluded

the model's representation for mass transfer from the condensed phase to the gas phase—namely, desorption/evaporation from a mechanically quiescent free surface—was deficient. Nonetheless, the effort to compare measurement and model-based results proved instructive. It revealed that the $k_j^g(T)$ values A&B had derived corresponded to maximum rates and were far from representative of the process as a whole. In addition, the investigation corroborated our suspicion that the $k_G^g(T, 11\text{ atm}) > k_G^g(T, 2\text{ atm})$ values A&B reported for the range 465 °C $\leq T \leq$ 530 °C could not be reproduced by a model predicated on pyrolysis products desorbing solely from a mechanically quiescent free surface. This led us to suspect the previously unexplored possibility that bubble-promulgated mass transfer played an important role in the experiments. It also seems possible that the Pt filament A&B employed to heat the samples could have catalyzed the process.

Because the process by which R45M pyrolysis products gasified in the T-jump experiments appeared to have been different in a significant way from the model we formulated to represent it, the comparisons of measurement-based and model-predicted results had limited value with respect to validating the theoretical framework we have proposed for modeling condensed-phase reaction chemistry. Nonetheless, results produced by the model did corroborate A&B's conclusion that the gasified products of R45M's pyrolysis at high heating rates would predominantly be "higher molecular weight fragments" that A&B broadly classified as oligomers of butadiene. As such, the study increased our confidence in the validity of the paradigm we have been employing for modeling R45M's deflagration in applications of interest.

To further evaluate the paradigm's validity for modeling R45M's deflagration in OFDF experiments and SFRJ combustors, we produced estimates for the temperature transients to which a subsurface layer of R45M would be subject as it evolved toward the surface of strands burning in the former. Those transients, in turn, were employed as bases for simulations to predict the degree to which EODT would decompose when subject to them. At the low end of (linear) burning rates reported by collaborators, less than 15% of the starting mass of EODT was decomposed by the end of the transient, and the percentages were lower at higher burning rates. As such, the study increased our conviction that EODT is more representative of the nascent gas-phase products at R45M's surface in OFDF experiments than a light hydrocarbon such as 1,3-butadiene or ethylene. Moreover, since burning rates are expected to be higher in SFRJ combustors, that conviction extends to CFD models for simulating their dynamics as well.

7. References

Arisawa H, Brill TB. Flash pyrolysis of hydroxyl-terminated polybutadiene (HTPB) I. Analysis and implications of the gaseous products. Combustion and Flame. 1996a;106:131–143.

Arisawa H, Brill TB. Flash pyrolysis of hydroxyl-terminated polybutadiene (HTPB) II. Implications of the kinetics to combustion of organic polymers. Combustion and Flame. 1996b;106:144–154.

Bouck LS, Baer AD, Ryan NW. Pyrolysis and oxidation of polymers at high heating rates. Fourteenth Symposium (International) on Combustion. 1973;14:1165–1176.

Brill TB. Surface pyrolysis phenomena and flame diagnostics by FTIR spectroscopy. International Journal of Energetic Materials and Chemical Propulsion. 1994;3:191–208.

Cai W, Thakre P, Yang V. A model of AP/HTPB composite propellant combustion in rocket motor environments. Combustion Science and Technology. 2008;180:2143–2169.

Chen JK, Brill TB. Chemistry and kinetics of hydroxyl-terminated polybutadiene (HTPB) and diisocyanate-HTPB polymers during slow decomposition and combustion-like conditions. Combustion and Flame. 1991;87:217–232.

Chen C-C, McQuaid MJ. Thermochemical and kinetic studies of the pyrolysis of hydroxyl-terminated polybutadiene (HTPB). Presented at the 35th JANNAF Propellant and Explosives Characterization Subcommittee Meeting; 2009.

Chen C-C, McQuaid MJ. Thermochemistry and kinetics modeling of hydroxyl-terminated polybutadiene-red fuming nitric acid (HTPB-RFNA) systems. Presented at the 5th JANNAF Liquid Propulsion Subcommittee Meeting; 2010.

Chen C-C, McQuaid MJ. Thermochemical and kinetics modeling pertaining to AP-HTPB composite propellant combustion. Presented at the 39th JANNAF Propellant and Explosives Characterization Subcommittee Meeting; 2015.

Chen C-C, McQuaid MJ. Thermochemical and kinetics modeling of the oxidation of hydroxyl-terminated polybutadiene in air. Presented at the 44th JANNAF Combustion Subcommittee Meeting; 2011.

Chen C-C, McQuaid MJ. A skeletal finite rate chemical kinetics mechanism for modeling HTPB-air combustion in a gun-launched solid-fuel ramjet combustor. Army Research Laboratory (US); 2020. Report No.: ARL-TR-8891.

Chen C-C, McQuaid MJ, Stone C, Veals JD. Addendum to ARL-TR-2681. On modeling the pyrolysis of hydroxyl-terminated polybutadiene (HTPB) type R45M at temperatures in the range 465–600 °C. DEVCOM Army Research Laboratory (US); 2023. Report No.: ARL-TN-1155.

Chirico RD, Nguyen A, Steele WV, Strube MM. Vapor pressure of n-alkanes revisited. New high-precision vapor pressure data on n-decane, n-eicosane, and n-octacosane. J Chem Eng Data. 1989;34:149–156.

Dennis CN. Email communication. Naval Air Warfare Center Weapons Division; 2022 Mar 9.

Du TF. Thermal-decomposition studies of solid-propellant binder HTPB. Thermochim Acta. 1989;138:189–197.

Ericsson I. Sequential pyrolysis gas chromatographic study of the decomposition kinetics of cis-1,4-polybutadiene. Journal of Chromatographic Science. 1978;16:340–344.

Ganesh K. Primary pyrolysis products of hydroxy-terminated polybutadiene. Macromolecules. 2000;33:326–330.

Geipel CM, Bojko BT, Pfützner CJ, Fisher BT, Johnson RF. Regression of solid polymer fuel strands in opposed-flow combustion with gaseous oxidizer. Proceedings of the Combustion Institute. 2022;1–11.

Gross ML. Two-dimensional modeling of AP/HTPB utilizing a vorticity formulation and one-dimensional modeling of AP and ADN [dissertation]. Brigham Young University; 2007.

Lu YC, Kuo KK. Thermal decomposition study of hydroxyl-terminated polybutadiene (HTPB) solid fuel. Thermochimica Acta. 1996;275:181–191.

McDonald AJ, Baier MJ, Son SF, McQuaid MJ, Chen CC, Veals JD, Stone CP, Goldenstein CS. Laser absorption measurements of temperature and CO profiles in opposed-flow diffusion flames of solid propellants. 13th US National Combustion Meeting. 2023.

McQuaid MJ, Chen C-C, Drake GW. An analysis pertaining to temperature gradients in deflagrating ammonium perchlorate particles. Army Research Laboratory (US); 2015. Report No.: ARL-TR-7403.

McQuaid MJ, Chen C-C, Veals JD, Yeh I-C. Detailed finite-rate chemical kinetics-based modeling of nitroglycerin in systems comprising liquid and gas phases. Presented at the 43rd JANNAF Propellant and Explosives Development and Characterization Subcommittee Meeting; 2021.

McQuaid MJ, Chen C-C, Veals JD. Simulating accelerating rate calorimetry experiments with a model having a detailed, gas-phase, finite-rate chemical kinetics mechanism: results for RDX. Presented at the 40th JANNAF Propellant and Explosives Development and Characterization Subcommittee Meeting; 2017.

McQuaid MJ, McNesby KL, Rice BM, Chabalowski CF. Density functional theory characterization of the structure and gas-phase mid-infrared absorption spectrum of 2-azido-N,N-dimethylethanamine (DMAZ). Journal of Molecular Structure (THEOCHEM). 2002;587:199–218.

McQuaid MJ, Miziolek AW, Sausa RC, Merrow CN. Photodissociation of dimethylnitramine at 248 nm. Journal of Physical Chemistry. 1991;95:2713–2718.

McQuaid MJ, Veals J, Yeh IC, Chen C-C. The development of detailed finite-rate chemical kinetics mechanisms for modeling decomposition in condensed phases. Part 2. The parameterization of free volume theory for liquid nitrate esters. Presented at the 50th JANNAF Combustion Subcommittee Meeting; 2020.

Miller MS. Three-phase combustion modeling: frozen ozone, a prototype. Army Research Laboratory (US); 1997. Report No.: ARL-TR-1320.

Myers CG, Munns GW. Platinum hydrocracking of pentanes, hexanes, and heptanes. Ind Eng Chem. 1958;12:1727–1732.

Nusca MJ. Computational modeling of gun-launched solid fuel ramjet (SFRJ) projectile-regression rate and chemical kinetics studies. Proceedings of the 51st JANNAF Combustion Subcommittee Meeting; 2022

Nusca MJ, Chen C-C, McQuaid MJ. Modeling and combustion chamber dynamics of two selectable thrust rocket motor concepts. Proceedings of the High-Performance Computing Modernization Program Users Group Conference; 2011.

Nusca MJ, Minnicino M, Chen CC, Isert S, McBain A. Multidisciplinary gun-launched solid fuel ramjet (SFRJ) projectile study – initial CFD modeling results. Presented at the 49th JANNAF Combustion Subcommittee Meeting; 2019.

Sandall ET, Kalman J, Quigley JN, Munro S, Hedman TD. A study of solid ramjet fuel containing boron-magnesium mixtures. Propulsion and Power Research. 2017;6:243–252.

Stein SE, Brown RL. Estimation of normal boiling points from group contributions. J Chem Inf Comput Sci. 1994;34:581–587.

Tummers B. DataThief III [accessed 2023 Feb 6]. https://datathief.org/2006.

Varney AM, Strahle WC. Thermal decomposition studies of some solid propellant binders. Combustion and Flame. 1971;16:1–7.

Veals JD, Yeh IC, Chen C-C, Andzelm J, McQuaid MJ. Establishing and parameterizing rate coefficient functions for steps in the decomposition of nitrate esters in condensed phases: progress in the development of a practical approach. Presented at the 41st JANNAF Propellant and Explosives Development and Characterization Subcommittee Meeting; 2018.

Veals JD, Chen C-C, McQuaid MJ. Recent advances in modeling RDX combustion kinetics. Presented at the 49th JANNAF Combustion Subcommittee Meeting; 2019.

Weast RC, Grasselli JG, eds. CRC handbook of data on organic compounds, 2nd Ed. CRC Press, Inc.; 1989.

Wingard ZK, Thompson DM, Simmons EL. Tactical Army hybrid-propulsion development. Proceedings of the 5th JANNAF Liquid Propulsion Subcommittee Meeting, Chemical Propulsion Information Analysis Center, CPIAC Publication JSC CD-62; 2010.

Zeldovich YB. On the theory of combustion of powders and explosives. J Exp Theor Phys. 1942;12:498–524.

List of Symbols, Abbreviations, and Acronyms

A&B	Arisawa and Brill
Ar	argon
ARL	Army Research Laboratory
C	carbon
C2H4	ethylene
C4H6	1,3-butadiene
CFD	computational fluid dynamics
DEVCOM	US Army Combat Capabilities Development Command
DME	dimethylether
DOD	US Department of Defense
EODT	6-ethenyl-2,8,12,16-octadecetetraene
FTIR	Fourier transform infrared
H	hydrogen
HH	hypergolic hybrid
HLK	Hertz–Langmuir–Knudsen
HR	homogeneous reactor
HTPB	hydroxyl-terminated polybutadiene
IR	infrared
MEP	minimum energy path
O_2	oxygen
OFDF	opposed-flow diffusion flame
Pt	platinum
RFNA	red fuming nitric acid
SFRJ	solid-fuel ramjet

1 (PDF) DEFENSE TECHNICAL INFORMATION CTR
DTIC OCA

1 (PDF) DEVCOM ARL
FCDD RLB CI
TECH LIB

12 (PDF) DEVCOM ARL
FCDD RLA WA
N TRIVEDI
E BYRD
B BARNES
R PESCE-RODRIGUEZ
FCDD RLA WC
M MCQUAID
C-C CHEN
C STONE
M MINNICINO
R CORNELL
M NUSCA
FCDD RLD CD
J VEALS
FCDD RLR A
J CIEZAK

5 (PDF) US NAVAL RESEARCH LABORATORY
B BOJKO
T LOEGEL
CJ PFUZNER
IV SCHWEIGERT
A EPSHTEYN

1 (PDF) NAVAL AIR WARFARE CENTER WEAPONS DIVISION
C DENNIS

2 (PDF) PURDUE UNIVERSITY
C GOLDENSTEIN
S SON